# Infiltration of Supermicron Aerosols into a Simulated Space Telescope

February 10, 2011

De-Ling Liu and Kenneth T. Luey
Space Materials Laboratory
Physical Sciences Laboratories

Prepared for:

Space and Missile Systems Center
Air Force Space Command
483 N. Aviation Blvd.
El Segundo, CA 90245-2808

Authorized by: Engineering and Technology Group

# 20110613179

**⬠ AEROSPACE**
*Assuring Space Mission Success*

David E. Davis
SMC/EA

# REPORT DOCUMENTATION PAGE

| 1. REPORT DATE (DD-MM-YYYY) | 2. REPORT TYPE | 3. DATES COVERED (From - To) |
|---|---|---|
| 10-02-2011 | | |

| 4. TITLE AND SUBTITLE | 5a. CONTRACT NUMBER |
|---|---|
| Infiltration of Supermicron Aerosols into a Simulated Space Telescope | FA8802-09-C-0001 |
| | 5b. GRANT NUMBER |
| | 5c. PROGRAM ELEMENT NUMBER |

| 6. AUTHOR(S) | 5d. PROJECT NUMBER |
|---|---|
| De-Ling Liu and Kenneth T. Luey | 5e. TASK NUMBER |
| | 5f. WORK UNIT NUMBER |

| 7. PERFORMING ORGANIZATION NAME(S) AND ADDRESS(ES) | 8. PERFORMING ORGANIZATION REPORT NUMBER |
|---|---|
| The Aerospace Corporation<br>Physical Sciences Laboratories<br>El Segundo, CA 90245-4691 | TR-2011(8550)-1 |

| 9. SPONSORING / MONITORING AGENCY NAME(S) AND ADDRESS(ES) | 10. SPONSOR/MONITOR'S ACRONYM(S) |
|---|---|
| Space and Missile Systems Center<br>Air Force Space Command<br>483 N. Aviation Blvd.<br>El Segundo, CA 90245 | SMC |
| | 11. SPONSOR/MONITOR'S REPORT NUMBER(S) |

**12. DISTRIBUTION/AVAILABILITY STATEMENT**

Approved for public release; distribution unlimited.

**13. SUPPLEMENTARY NOTES**

**14. ABSTRACT**

Purging is a common scheme to protect sensitive surfaces of payloads and spacecraft from airborne contaminant intrusion during ground assembly, integration, and launch vehicle encapsulation. However, the purge for space volumes must be occasionally interrupted. Thus, it is important to gain insights into the transport of ambient particles penetrating through vent holes and entering the interior of a confined space system, such as a space telescope, during a purge outage. This study presents experimental work performed to measure time-dependent aerosol concentration changes during a purge outage. The laboratory results from the aerosol experiments were compared with a mass balance-based mechanistic model that had been experimentally validated for aerosols ranging from 0.5 to 2 μm. The experimental data show that the steady-state aerosol concentration inside a simulated space telescope (SST) is governed by the surrounding particle concentration, SST air exchange rate, and the particle deposition rate.

**15. SUBJECT TERMS**

Particulate infiltration, Intrusion, Space telescope

| 16. SECURITY CLASSIFICATION OF: | | | 17. LIMITATION OF ABSTRACT | 18. NUMBER OF PAGES | 19a. NAME OF RESPONSIBLE PERSON |
|---|---|---|---|---|---|
| a. REPORT | b. ABSTRACT | c. THIS PAGE | Leave blank | 17 | De-Ling Liu |
| UNCLASSIFIED | UNCLASSIFIED | UNCLASSIFIED | | | 19b. TELEPHONE NUMBER (include area code)<br>(310)336-0062 |

# Acknowledgments

# Contents

# Figures

## Tables

# 1. Introduction

Inert gas or air purging is widely implemented to prevent airborne contaminants from infiltrating into confined space systems during testing, integration, and launch vehicle encapsulation. However, purges are often turned off, either by processing plan or by inadvertent actions. In the aerospace contamination control community, empirical correlations developed by Buch and Barsh,[1] and Hamberg[2] are used to perform payload purge outage analysis in order to establish appropriate purge outage requirements. Alternatively, the transport of particles can be predicted by parameters that characterize air exchange rate and particle deposition rate inside the space system volumes. The work described in this report presents measurements of time-dependent infiltration of supermicron airborne particle infiltration into a simulated space telescope (SST), where "supermicron" means particles with aerodynamic diameter greater than 1 $\mu$m. The results are compared with a mechanistic model developed in previous work.[3]

For particulate contamination relevant to space systems, supermicron particles are of greatest concern because effects of contamination such as percent area coverage (PAC) or obscuration are most impacted by particles in this size range.[4] The experimental results presented here provide a dynamic picture of supermicron airborne particle intrusion into an enclosed space volume once the purge is turned off. In this report, the terms "aerosols" and "airborne particles" are used interchangeably since their definitions are "a suspension of solid or liquid particles in a gas."[5]

1

## 2. Background

Development of a mechanistic model based on mass balance for predicting airborne particle infiltration into an SST was described previously.[3] Here, we present a brief summary.

After the purge is turned off, the airborne particle concentration change as a function of time inside the SST can be represented by the following equation:

$$\frac{dC_{SST}}{dt} = \lambda C_c - (\lambda + k)C_{SST}$$

(1)

where $C_{SST}$ and $C_c$ are the airborne particle number concentrations inside the SST and in the chamber (mass/cm$^3$ or #/cm$^3$), respectively; $\lambda$ and $k$ are the air-exchange rate (Volume Air Changes per Hour, ACH, h$^{-1}$) and particle deposition rate (h$^{-1}$) onto the SST interior surfaces, respectively. The air-exchange rate is defined as the ratio of air flowrate ($Q$) into, or out of, the enclosure volume ($V$) under isothermal conditions in which the air volume does not expand or contract, i.e., ACH = $Q/V$. Note that the particle deposition coefficient, $k$, is a function of particle size. Thus, one should expect that the extent of particle concentration growth due to infiltration would vary according to particle sizes.

Equation (1) states that the rate of airborne particle concentration change inside the SST is governed by a *source* term, $\lambda C_c$, and a *sink* term, $(\lambda + k)C_{SST}$. Assuming $C_c$, $\lambda$, and $k$ are constant over time, and the initial aerosol concentration inside the control volume is zero (i.e., $C_{SST} = 0$ at $t = 0$), the time-dependent particle concentration inside the SST, $C_{SST}(t)$, can be expressed as the analytical solution to Eq. (1):

$$C_{SST}(t) = \frac{\lambda}{\lambda + k}C_c\left[1 - \exp(-(\lambda + k)t)\right]$$

(2)

After rearrangement, Eq. (2) becomes

$$\frac{C_{SST}(t)}{C_c} = \frac{\lambda}{\lambda + k}\left[1 - \exp(-(\lambda + k)t)\right]$$

(3)

For sufficiently large values of $t$, the steady-state concentration can be estimated as

$$C_{SST} = \frac{\lambda}{\lambda + k}C_c$$

(4)

or

$$\frac{C_{SST}}{C_c} = \frac{\lambda}{\lambda + k}.$$ (5)

At steady state, the airborne particles brought into the SST from exterior ambient air ($\lambda C_c$, the *source* term) are balanced by airborne particle loss inside the SST due to deposition onto the surfaces ($kC_{SST}$) and air exfiltration that removes the particles ($\lambda C_{SST}$). The experimental approach therefore involves measurement of $C_c$ and $C_{SST}$. In previous work, the measurements of $C_c$ and $C_{SST}$ were achieved using the natural ambient aerosol population in typical rooms. In room air, the concentration of airborne particles with aerodynamic diameters larger than 2 µm is not sufficient for the experiments. The work described in this report uses a new, atomizing source to generate particles larger than 2 µm in a wider size range.

In addition to $C_c$ and $C_{SST}$, the SST air-exchange rate, $\lambda$, is also needed for providing inputs in the analysis. The air-exchange rate is characterized as the rate of air replenishment within an enclosed volume by outside "fresh air." It is not feasible to directly measure the air flowrate when air enters or leaves the enclosure volume through uncontrolled leaks. Therefore, a tracer gas technique is employed to determine the air-exchange rate. To measure the air-exchange rate, a uniform concentration of tracer gas is established throughout the volume by a brief pulse injection of tracer gas into the enclosure. Once the tracer gas pulse has been depleted, its concentration is diluted over time due to air replenishment from outside ambient air. The ambient air preferably contains no presence of tracer gas, or a low, stable, background concentration of tracer gas. The rate of tracer gas concentration change within the enclosed volume is given by

$$\frac{dC}{dt} = -\lambda C,$$ (6)

where $C$ is the tracer gas concentration. After rearrangement, the solution to Eq. (6) becomes

$$\ln C(t) - \ln C(0) = -\lambda t,$$ (7)

where $C(0)$ and $C(t)$ are the tracer gas concentrations inside the SST at time $t = 0$ and $t$, respectively. When the air is well-mixed, plotting $\ln C$ as a function of time gives rise to a linear plot with the slope yielding the air-exchange rate $\lambda$.

# 3. Methods

## 3.1 Experimental Setup

The experimental work described here parallels the work described in Ref. 3. However, several significant changes have been made, as described in this Section. A new SST has been constructed and is described in Subsection 3.1.1. Most significantly, the airborne particle samples are produced by a controlled atomization process, giving a wider size range of particles at much higher concentrations. The aerosol atomizer is described in Subsection 3.1.2. To increase control of the particle population, the airborne concentration measurements are performed in a sealed chamber described in Subsection 3.1.3. The experimental measurement procedures for airborne concentrations and air-exchange rate are discussed in Subsections 3.1.4 and 3.1.5, respectively.

### 3.1.1 Simulated Space Telescope

A simulated space telescope (SST) was designed and constructed using aluminum sheets (20 mil thickness). The schematic diagram is shown in Figure 1. The extent of closure achieved by the front cover may be adjusted, but for all of the experiments discussed in this report, the SST was closed by making a full contact seal between the cover and the SST body. Although the cover is completely closed for these experiments, Figures 1 and 2 suggest that there are other leak areas caused by bulkhead feedthroughs and unwelded seams and joints. Thus, it is expected that the transport of air and airborne particles take place through the leakage paths. A fan is installed inside the SST to promote air mixing during air-exchange rate measurements.

### 3.1.2 Supermicron Aerosol Generator or Atomizer

Supermicron airborne particles were generated using a custom-built aerosol atomizer, shown schematically in Figure 2. The airborne particles generated from the atomizer comprise a wide particle size range (so-called "polydiserse") up to 10 μm in aerodynamic diameter. A saturated NaCl solution and compressed air (>50 psi) were simultaneously supplied into the nozzle to generate mists or droplets. The droplets, containing NaCl and water, were immediately desiccated by upward dry air in the column, leaving NaCl as the particles after water evaporates away from the droplet surface on the time scale of ms.[5] Since the percentage of NaCl in the droplets is proportional to the NaCl concentration in the solution fed into the atomizer, a saturated NaCl solution was used to produce the greatest size possible of eventual NaCl particles. Particles generated via atomizing processes carry surface charges on particle surfaces, thus a Kr-85 neutralizer (Model 3054, TSI Inc.,) was employed to neutralize the surface charges before aerosols were introduced into the chamber.

5
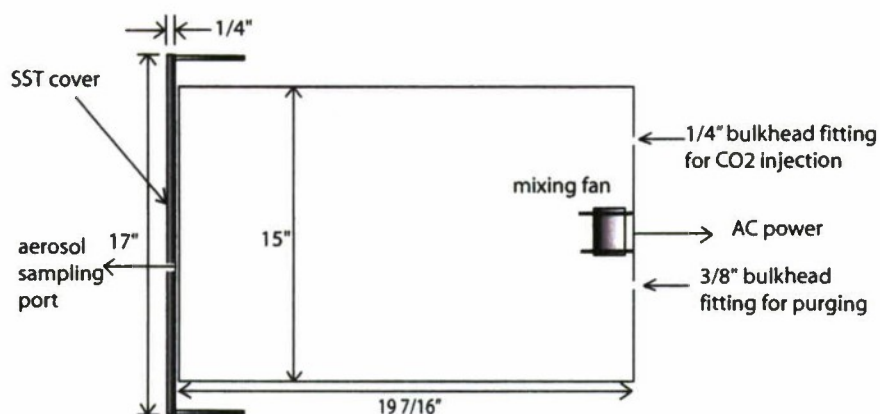
Figure 1.   Side view schematic of the simulated space telescope (SST) apparatus.
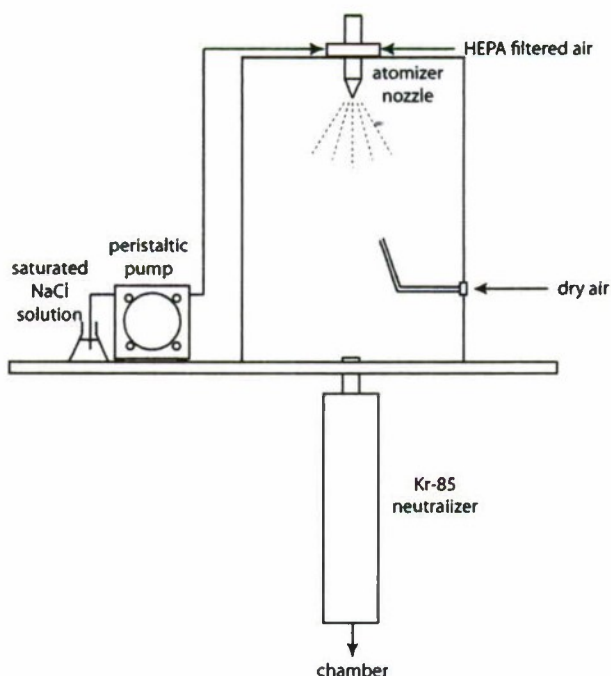


Figure 2.   Schematic of the custom-built aerosol atomizer used to
generate supermicron airborne particles.

### 3.1.3    Environmental Control Chamber

The SST is housed in an environmental control chamber (or "chamber" hereafter), as shown in Figure 3.  The chamber (4 x 4 x 4 ft$^3$) is constructed with ¼-in.-thick aluminum plates.  A fan used to mix air inside the chamber is located 20 cm below the ceiling panel in the center position.  The fan speed can be adjusted by varying the input voltage.  The fan inside the chamber provides spatially homogeneous airborne particle concentrations throughout the chamber so that samples collected from one location are representative of the entire chamber in terms of airborne particle concentrations.
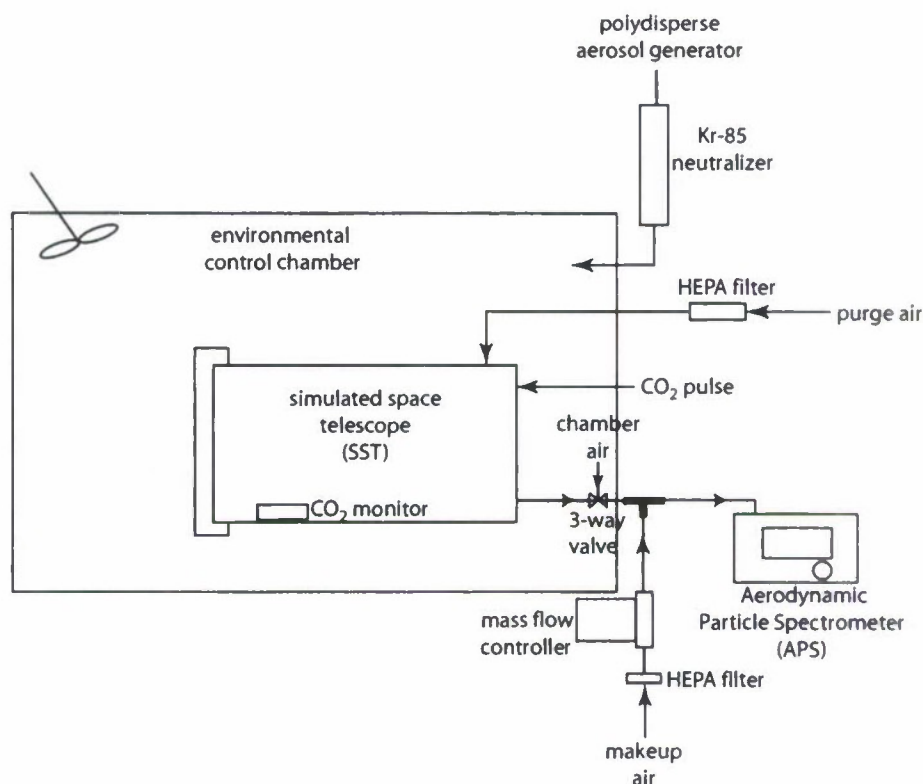
Figure 3.  Experimental schematic for measuring supermicron particle infiltration into a simulated space telescope (SST).

### 3.1.4    Aerosol Sampling and Measurements

Measurements of particle aerodynamic diameter and concentration were performed using an Aerodynamic Particle Spectrometer (APS, Model 3321, TSI Inc.,).  The APS provides real-time and highly size-resolved aerosol measurements from 0.5 to 20 μm over 52 channels.  Using an internal pump, the nominal aerosol flowrate into the APS is 1 L/min.  Filtered, particle-free makeup air (HEPA capsule, Pall Life Sciences) at 0.8 L/min regulated with a mass flow controller (MKS Instruments, Inc.) is supplied to the APS so that a 0.2 L/min aerosol flowrate is withdrawn to the APS from the chamber and SST, respectively.

In order to collect representative aerosol samples from the SST, where convection is the dominant mechanism for aerosol infiltration, a low aerosol sampling flow rate and a short sampling duration are highly desirable to minimize air perturbations inside the SST.  Additionally, a 3-way solenoid valve (ASCO Valve, Inc.) was in place so that the aerosol concentrations in the chamber, $C_c$, and that inside the SST, $C_{SST}$, can be measured sequentially.  The tubing diameters and lengths for sampling $C_c$ and $C_{SST}$ were made identical so that the corresponding aerosol loss in both sampling lines was the same.  This is particularly important for sampling supermicron aerosols because gravity is the dominant mechanism for particle loss within the sampling line.  Differences in the sampling line diameter, length, and orientation will lead to measurement errors in terms of the true $C_{SST}/C_c$ ratios for the system.

7

A LabView program was written to control APS aerosol sampling sequences and the valve switching in the laboratory experiments. Aerosol sampling duration, the sampling interval, and sampling line purge time were variables controlled by the program.

### 3.1.5    Air-Exchange Rate Measurements

The SST air-exchange rate was measured using a tracer gas technique, and $CO_2$ was used as the tracer gas in this study. A short pulse of $CO_2$ was generated from a $CO_2$ gas cylinder (Scott Specialty Gases) connected to the SST with tubing through a bulkhead fitting on the chamber wall. After $CO_2$ injection, the fan inside the SST was immediately turned on for 3 s for mixing. Two $CO_2$ monitors (Telaire 7001, Engelhard), one inside the SST and one in the chamber, were used to measure $CO_2$ concentration changes with time, as the $CO_2$ concentration flowing from the chamber into the SST may not be constant over the course of the experiment. Note that when $CO_2$ is used as a tracer gas for air-exchange rate calculations, the background $CO_2$ concentration in the chamber must be subtracted from the measured values prior to evaluating the $CO_2$ concentration decay rate.

# 4. Results and Discussion

## 4.1    Air-Exchange Rate Results

Measurements of the air-exchange rate, $\lambda$, were performed as discussed in Sections 2 and 3.1.5. During these measurements, the SST front cover was in direct physical contact with the opening, considered the fully closed configuration. Figure 4 shows the measured $CO_2$ concentrations inside the SST and in the chamber as a function of time. The $CO_2$ monitor has a detection limit at 2500 ppm, as indicated in Figure 4. In the experiments, the data points collected below 2500 ppm are sufficient to determine the ACH based on the decay rate of $CO_2$ concentration in the SST. Figure 4 illustrates the $CO_2$ concentration profile as a function of time from the air-exchange rate measurements when the chamber fan was set at high speed, and a linear regression was performed to calculate the slope, which yielded the air-exchange rate $\lambda$, as shown in Figure 5.

As shown in Table 1, the air-exchange rates determined from the tracer gas experiments were 3 $h^{-1}$ and 6 $h^{-1}$ for the low and high chamber fan speed settings, respectively. Previously, the experimental data indicated that the level of air turbulence adjacent to SST plays a role in affecting the air-exchange rate of the confined enclosure.[3] A higher degree of turbulence is expected to create stronger air convection in the chamber, which, in turn, enhances the mass transfer process by bringing the airborne particles into the SST from outside.
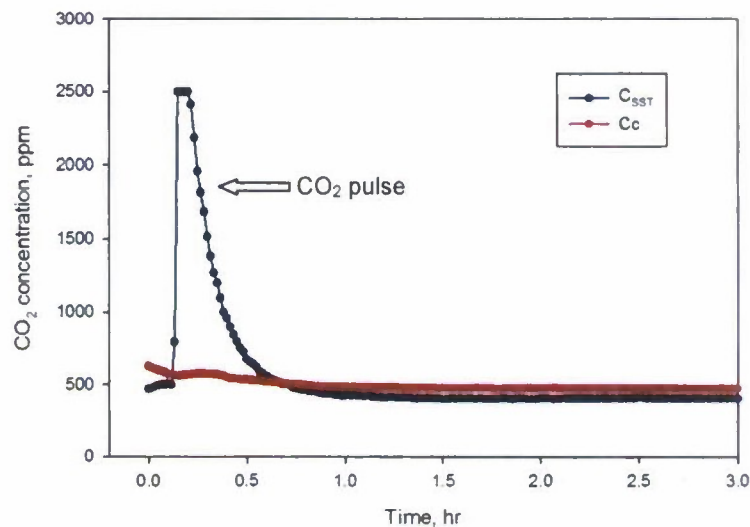


Figure 4.    $CO_2$ concentration profiles of the simulated space telescope and the chamber during the tracer gas experiment. The chamber fan was at a high-speed setting.
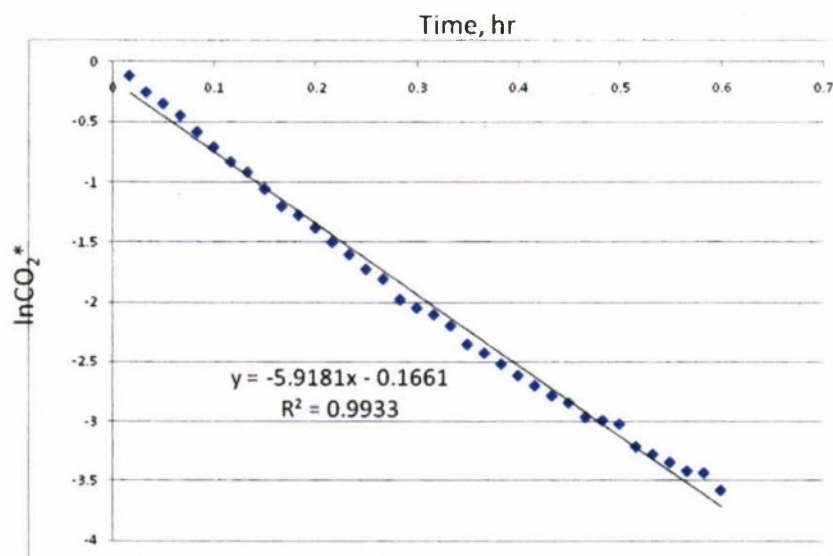
Figure 5. Air-exchange rate measured by $CO_2$ concentration decay in the simulated space telescope. The $CO_2$ concentration $C^*$ is background corrected as $C^* = [(CO_{2(t)} - CO_{2,b})/(CO_{2(0)} - CO_{2,b})]$, where $CO_{2,b}$ is the background $CO_2$ concentration in the experiments, which may vary slightly from run to run depending on human occupancy conditions.

Table 1. Air-Exchange Rates (ACH) Inside the SST Measured by the $CO_2$ Tracer Gas Technique under Different Fan Speed Settings and Aerosol Sampling Activities.[†] The SST was in a fully closed configuration.

| Fan Speed Settings | Air-Exchange Rate ($h^{-1}$) |
|---|---|
| High | 6 |
| Low | 3 |
| Low[*] | 1.5 |

[†] The aerosol samples from the SST were collected via the APS internal pump at every 6–7 min, with a flowrate of 0.2 L/min. The purge time for the sampling line is 10 s.

[*] No aerosol sampling

In addition to forced convection outside the SST (induced by chamber fan mixing), forced convection inside the SST caused by air volume displacement also contributes to increases in air-exchange rate. The example here is the active pumping for aerosol sampling. To examine this effect, tracer gas experiments were performed under the same conditions, but with no aerosol sampling. Under this scenario, the measured air-exchange rate was 1.5 $h^{-1}$, as compared to 3 $h^{-1}$ with aerosol sampling at the same low chamber fan speed. This indicates that air movement induced by active pumping inside the SST increases the infiltration of air flow, and airborne contaminants from outside of the enclosure. The $CO_2$ monitor, equipped with a small motor to continuously bring air samples into the device for measurements, is also expected to play a role in enhancing convection, thus increasing rate of infiltration.

In summary, air-exchange rates characterize the overall rate of air replenishment through all leaks and openings (either intentional or uncontrolled) of an enclosure volume. As a result, detailed information on the geometry of the leakage paths is not required. Air-exchange rates in a confined space volume are determined by the following factors: (1) leakiness of the enclosed volume, (2) the surround-

10

ing air turbulence level, (3) air movement inside the space volume caused by forced convection (continuous air input, turbulent mixing by mechanical mechanisms, such as fan stirring), and natural convection (the presence of thermal gradients). This work and our prior test data[3] have supported the above statements.

## 4.2    Supermicron Aerosol Output

The supermicron aerosol size distribution and concentrations were measured by the APS. Figure 6 compares airborne particles generated by the custom-built atomizer with room air. The atomizer produces aerosols with larger sizes (up to 10 μm) and at much higher concentrations than the airborne particles present in the room air. The ambient room air contains very low concentrations of airborne particles above 2 μm because they are more readily removed from the air due to gravitational settling.[5,6] The supermicron atomizer supplies sufficiently high concentrations of airborne particles to allow statistically reliable measurements of $C_{SST}/C_c$.

## 4.3    Particle Measurements

Particle infiltration experiments were conducted with the SST in a fully closed configuration. Airborne particles infiltrate into the SST through the uncontrolled leak paths such as the gap between the SST cover and the cylindrical volume, plumbing feedthroughs, and unwelded seams and joints.

Figure 7 illustrates the growth of aerosol concentration, $C_{SST}$, as a function of time for two different chamber fan speeds. A higher air-exchange rate is responsible for reaching steady state more rapidly for smaller particles (1–3 μm in diameter, as shown in ○ and □). On the other hand, there is no distinct difference in the characteristic time for establishing the steady state when particles are larger. This is because the characteristic time to reach steady state, τ, can be approximated as
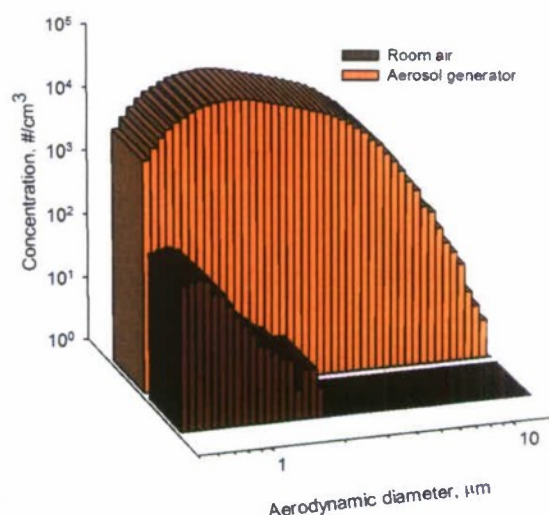


Figure 6.    Comparison of aerosol size distribution and concentration from the supermicron aerosol atomizer to the airborne particles in ambient room environment.
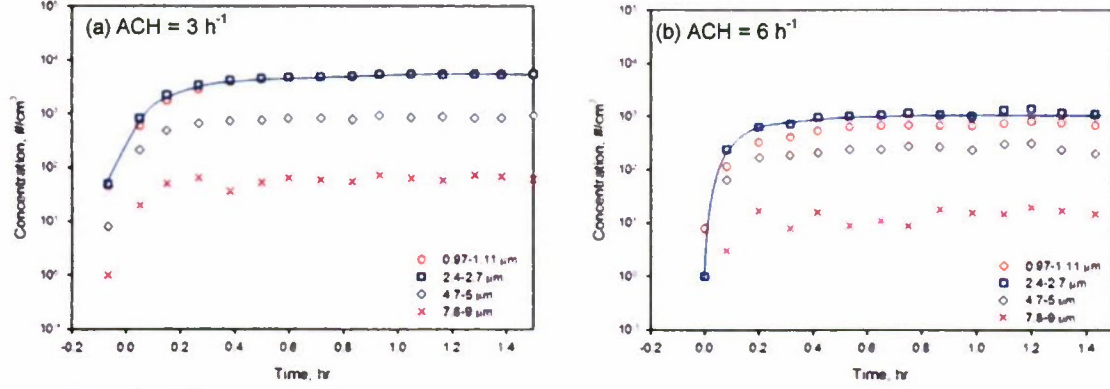
Figure 7. The concentration growth of airborne particles inside SST, $C_{SST}(t)$, after the purge was turned off in the experiments under different degrees of turbulence inside the chamber. The experimentally measured air-exchange rates were 3 and 6 h$^{-1}$, respectively for (a) and (b).

$$\tau \sim \frac{1}{\lambda + k},$$

(8)

where $k$ is the particle deposition rate. The value of $\lambda$ becomes more dominant to determine $\tau$ when $\lambda \gg k$, as discussed in our previous work,[3] and in Figures 8(a) and 8(b). The results from the supermicron aerosol experiments, as seen in Figures 7(a) and 7(b), are consistent with the modeling analysis and the laboratory work presented earlier, as illustrated in Figures 5 and 6 and Table 2 in Ref. 3.

## 4.4 Comparison of Experimental Data and Model Calculations

Particle infiltration experiments were conducted to compare with the modeling predictions. For all infiltration experiments, the SST was located in the chamber, and the SST air-exchange rate is governed primarily by the chamber fan speed and aerosol sampling actions. The air-exchange rates were measured simultaneously during particle infiltration processes. The ratios of $C_{SST}/C_c$ as a function of particle size were determined from $C_{SST}$ and $C_c$ measurements by the APS.

Figure 8 illustrates the comparison of modeling calculations and the laboratory results from the particle infiltration experiments. In the figure, different symbols were used to indicate the measured $C_{SST}/C_c$ ratios for different particle size ranges for the indicated ACH values. The curve fits were obtained from the model calculations as given in Eq. (3), and based on particle deposition rates, $k$, that yielded the best fit to the experimental data. It can be seen in Figure 8 that the experimental results compare reasonably well with the modeling analysis.

The values of $\lambda$ and $k$, and the characteristic times, $\tau$, for the airborne particles obtained from the above infiltration experiments are calculated and presented in Table 2.

Table 2 shows that large particles, due to their larger $k$ values, tend to reach steady state sooner as compared with smaller particles. This is true regardless of the air-exchange rate. On the other hand, $\tau$ for smaller particles is more strongly influenced by the air-exchange rate. A hypothetical example of 0.1 h$^{-1}$ air-exchange rate is provided in Table 2 for accentuation. We note that $\tau$ is quite short for a simulated telescope that is relatively low in leak area. A more realistic space telescope designed for ascent venting will reach steady state in a much shorter time after the purge is lost.

12
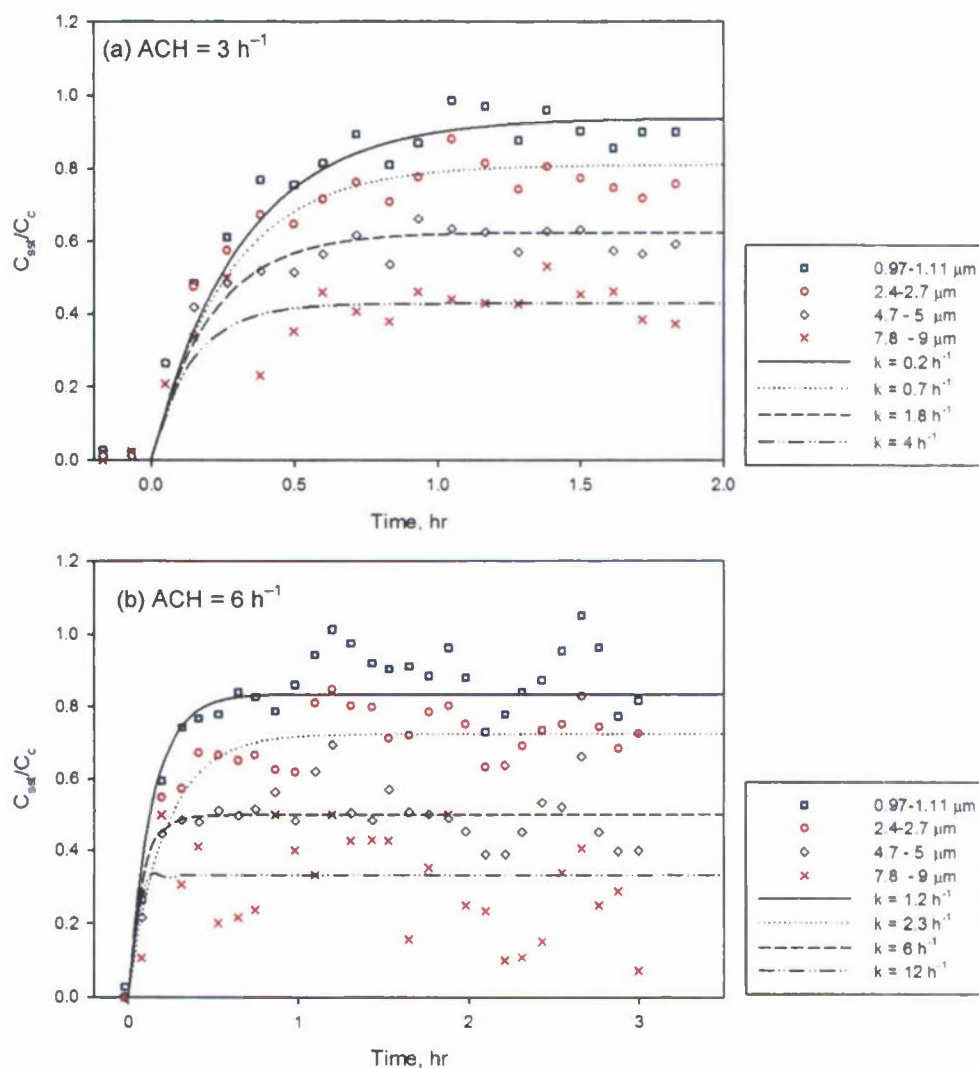
Figure 8. Comparison of modeling calculations with laboratory data in the SST particle infiltration experiments under two different ACH settings. The values of ACH were obtained using $CO_2$ tracer gas decay method.

Table 2. Characteristic Times and Particle Deposition Rates Obtained from the Aerosol Infiltration Experiments under Different Air-Exchange Rates

| Particle size, μm | $\lambda = 3\ h^{-1}$ | | $\lambda = 6\ h^{-1}$ | | $\lambda = 0.1\ h^{-1}$ (hypothetical) | |
|---|---|---|---|---|---|---|
| | $k, h^{-1}$ | $\tau, h$ | $k, h^{-1}$ | $\tau, h$ | $k, h^{-1}$ | $\tau, h$ |
| 0.97 – 1.11 | 0.2 | 0.31 | 1.2 | 0.14 | 0.2 | 3.33 |
| 2.4-2.7 | 0.7 | 0.27 | 2.3 | 0.12 | 0.7 | 1.25 |
| 4.7-5 | 1.8 | 0.21 | 6 | 0.08 | 1.8 | 0.53 |
| 7.8-9 | 4 | 0.14 | 12 | 0.06 | 4 | 0.24 |

Note that the $k$ values fit in the model calculations yield different particle deposition rates for different air-exchange rate conditions for the four particle size ranges studied here. Particle deposition

rates characterize the mass transfer processes of airborne particles onto surfaces (or airborne particles removal from the gas phase). Particle deposition rates are governed by particle sizes, air turbulence level, and surface characteristics (roughness, orientation, etc.).[7] For the same particle size, it has been well documented that increasing air turbulence levels lead to higher particle deposition rates.[6-8] This is because under higher air turbulence scenarios, airborne particles carried by eddy currents are more readily brought to the vicinity of the surface for subsequent deposition.[9] Therefore, higher $k$ values found in the higher air-exchange rate condition in this work are consistent with the experimental and theoretical findings in the literature.[6-7]

# 5. Conclusions

Laboratory work was conducted to investigate the dynamics of airborne particle transport into a generic confined space system volume. The experimental results were compared to a mechanistic model that takes into account particle transport processes by means of air exchange and particle deposition onto interior surfaces. Airborne particle concentration change inside a system volume is governed by two parameters: *air-exchange rate* (ACH) $\lambda$, and *particle deposition rate $k$*. The air-exchange rate was measured using a tracer gas technique, and the size-specific particle deposition rates were determined by fitting the experimental data to the analytical solution, as shown in Eq. (3).

The infiltration experiments were performed using supermicron airborne particles up to 10 $\mu$m under two ACH settings: 3 and 6 $h^{-1}$. The experimental data indicate that after the purge is off, the particle concentration increases with time until it reaches a steady state, which stays at a constant level relative to the ambient particle concentration. The rate of particle concentration increase can be approximated by the *characteristic time*, $\tau$, which is associated with $\lambda$ and $k$, as indicated in Eq. (8). The steady-state particle concentration inside the space volume, $C_{SST}$, is governed by $\lambda$, $k$, as well as the ambient concentration $C_c$, as shown in Eq. (4). The experimental data show a reasonable agreement with the model analytical results.

From a contamination control perspective, typical enclosed space systems, such as telescopes that are not launched under vacuum, must be designed to vent properly during ascent. The air-exchange rate of such systems is likely much higher than those studied here. It is thus critical to reduce $C_{SST}$ by controlling $C_c$ as much as possible. In addition, minimizing air-exchange rates in the space systems could be accomplished by reducing the air turbulence level surrounding the telescope. To establish physically based purge outage requirements, more efforts will be needed to characterize size-specific particle deposition rates under the air flow conditions representing the actual degree of turbulence inside space system volumes. Furthermore, particle fallout rates determined from such deposition experiments are expected to help elucidate the time-dependent correlation between air cleanliness class and surface particle cleanliness level.

# References

1.  Buch, J. D. and Barsh, M. K., Analysis of particulate contamination buildup on surfaces, *SPIE proceedings: optical system contamination: effect, measurement, control*, 1987, 777: 43–54.

2.  Hamberg, O., Particle fallout predictions for cleanrooms, *Journal of Environmental Science*, 1982, 25:15.

3.  Liu, D.-L. and Luey, K. T., Particulate infiltration into a simulated space telescope, *SPIE proceedings: optical system contamination: effect, measurement, control*, 2008, 7069, 706907-1.

4.  Tribble, A. C., *Fundamentals of Contamination Control*, SPIE Press, 2000, Bellingham, WA.

5.  Hinds, W. C., *Aerosol Technology: Properties, Behavior, and Measurement of Airborne Particles*, 1999, 2$^{nd}$ ed. John Wiley, New York.

6.  Lai, A. C. K., Particle deposition indoors: a review, *Indoor Air*, 2002, 12: 211-214.

7.  Liu, D.-L., Particle deposition onto enclosure surfaces, a chapter in *Developments in Surface Contamination and Cleaning*, edited by Kohli R. and Mittal K. L., 2010, Elsevier.

8.  Thatcher, T. L., Lai, A. C. K., Moreno-Jackson, R., Sextro, R. G., and Nazaroff, W. W., Effects of room furnishings and air speed on particle deposition rates indoors, *Atmospheric Environment*, 2002, 36: 1811-1819.

9.  Nazaroff, W. W., Gadgil, A. J., and Weschler, C. J., Critique of the use of deposition velocity in modeling indoor air quality, *Modeling of Indoor Air Quality and Exposure*, ASTM STP 1205 (N. L. Nagda, ed.), American Society for Testing and Materials, Philadelphia, 1993, 81-104.

# PHYSICAL SCIENCES LABORATORIES

The Aerospace Corporation functions as an "architect-engineer" for national security programs, specializing in advanced military space systems. The Corporation's Physical Sciences Laboratories support the effective and timely development and operation of national security systems through scientific research and the application of advanced technology. Vital to the success of the Corporation is the technical staff's wide-ranging expertise and its ability to stay abreast of new technological developments and program support issues associated with rapidly evolving space systems. Contributing capabilities are provided by these individual organizations:

**Electronics and Photonics Laboratory:** Microelectronics, VLSI reliability, failure analysis, solid-state device physics, compound semiconductors, radiation effects, infrared and CCD detector devices, data storage and display technologies; lasers and electro-optics, solid-state laser design, micro-optics, optical communications, and fiber-optic sensors; atomic frequency standards, applied laser spectroscopy, laser chemistry, atmospheric propagation and beam control, LIDAR/LADAR remote sensing; solar cell and array testing and evaluation, battery electrochemistry, battery testing and evaluation.

**Space Materials Laboratory:** Evaluation and characterizations of new materials and processing techniques: metals, alloys, ceramics, polymers, thin films, and composites; development of advanced deposition processes; nondestructive evaluation, component failure analysis and reliability; structural mechanics, fracture mechanics, and stress corrosion; analysis and evaluation of materials at cryogenic and elevated temperatures; launch vehicle fluid mechanics, heat transfer and flight dynamics; aerothermodynamics; chemical and electric propulsion; environmental chemistry; combustion processes; space environment effects on materials, hardening and vulnerability assessment; contamination, thermal and structural control; lubrication and surface phenomena. Microelectromechanical systems (MEMS) for space applications; laser micromachining; laser-surface physical and chemical interactions; micropropulsion; micro- and nanosatellite mission analysis; intelligent microinstruments for monitoring space and launch system environments.

**Space Science Applications Laboratory:** Magnetospheric, auroral and cosmic-ray physics, wave-particle interactions, magnetospheric plasma waves; atmospheric and ionospheric physics, density and composition of the upper atmosphere, remote sensing using atmospheric radiation; solar physics, infrared astronomy, infrared signature analysis; infrared surveillance, imaging and remote sensing; multispectral and hyperspectral sensor development; data analysis and algorithm development; applications of multispectral and hyperspectral imagery to defense, civil space, commercial, and environmental missions; effects of solar activity, magnetic storms and nuclear explosions on the Earth's atmosphere, ionosphere and magnetosphere; effects of electromagnetic and particulate radiations on space systems; space instrumentation, design, fabrication and test; environmental chemistry, trace detection; atmospheric chemical reactions, atmospheric optics, light scattering, state-specific chemical reactions, and radiative signatures of missile plumes.